Ideal Laser-Beam Propagation through High-Temperature Ignition Hohlraum Plasmas

D. H. Froula,* L. Divol, N. B. Meezan, S. Dixit, J. D. Moody, P. Neumayer, B. B. Pollock,† J. S. Ross, and S. H. Glenzer

L-399, Lawrence Livermore National Laboratory, P.O. Box 808, Livermore, California 94551, USA

(Received 12 October 2006; published 21 February 2007)

We demonstrate that a blue (3ω, 351 nm) laser beam with an intensity of 2×10^{15} W cm^{-2} propagates nearly within the original beam cone through a millimeter scale, $T_e = 3.5$ keV high density ($n_e = 5 \times 10^{20}$ cm^{-3}) plasma. The beam produced less than 1% total backscatter at these high temperatures and densities; the resulting transmission is greater than 90%. Scaling of the electron temperature in the plasma shows that the plasma becomes transparent for uniform electron temperatures above 3 keV. These results are consistent with linear theory thresholds for both filamentation and backscatter instabilities inferred from detailed hydrodynamic simulations. This provides a strong justification for current inertial confinement fusion designs to remain below these thresholds.

DOI: 10.1103/PhysRevLett.98.085001 PACS numbers: 52.38.−r, 52.25.Os, 52.35.Fp, 52.50.Jm

Inertial confinement fusion and high energy density science experiments at large laser facilities require efficient laser-beam propagation through long underdense plasmas to deposit energy at a desired region of interest. In the indirect drive approach to inertial confinement fusion (ICF), a high-Z radiation cavity (hohlraum) filled with a low density gas is used to convert laser energy into soft x-ray radiation to drive a fusion capsule implosion by ablation pressure [1]. For achieving a symmetric capsule implosion and for reaching ignition conditions, it is required that the energetic laser beams efficiently propagate through the interior of the hohlraum and create soft x rays close to where the laser beams were initially pointed on the hohlraum wall. The inside of the hohlraum will be filled with a low-Z or mid-Z long-scale length ($L \sim 2$–4 mm), high-temperature ($T_e \gg 3$ keV) plasma ranging in density from $n_e = 5 \times 10^{20}$ to $n_e = 15 \times 10^{20}$ cm^{-3} consisting of the initial fill material, ablated material off the capsule, and other lined hohlraum surfaces. The physics of laser-beam propagation in ignition hohlraums is largely dominated by the laser-plasma interactions in the fill plasma where laser backscattering, beam deflection, beam filamentation, and self-focusing may occur when driving these instabilities beyond their thresholds [2].

In this study, we present experiments that for the first time demonstrate transparent plasmas in high electron temperature ignition conditions. A 3ω (351 nm) laser beam with an intensity of 2×10^{15} W cm^{-2} propagates within the original beam cone through a millimeter scale, $T_e = 3.5$ keV, underdense ($n_e = 5 \times 10^{20}$ cm^{-3}) plasma. We show that increasing the electron temperature reduces the total backscatter. At a peak electron temperature of 3.5 keV, less than 1% total backscatter and a transmission greater than 90% is observed. The plasma conditions have been well characterized using Thomson scattering and the electron temperature is controlled by varying the total laser energy used to heat the target [3]. It is shown that reducing the electron temperature or increasing the intensity of the laser beam leads to filamentation and increased stimulated Brillouin scatter (SBS).

A new target platform [Fig. 1(a)] for studying laser-plasma interactions in 2-mm long high-temperature plasmas has been developed by aligning an interaction beam down the axis of a gas-filled gold cylinder (hohlraum); this allows direct measurements of the laser-beam propagation and transmission through ignition hohlraum plasmas. The hohlraum is heated by 33 1-ns square pulsed frequency tripled ($\lambda_0 = 351$ nm) laser beams at the Omega Laser

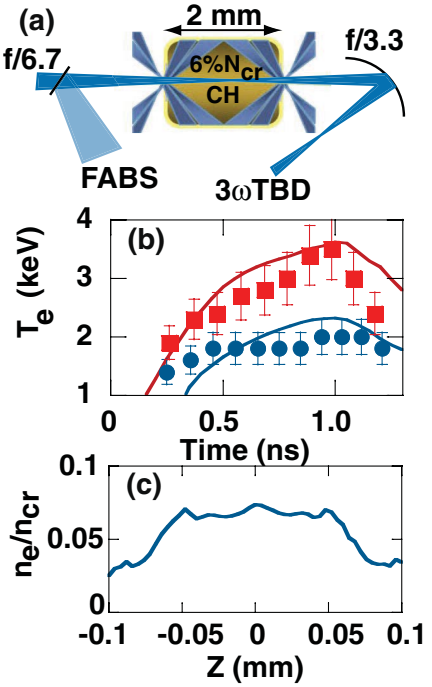

FIG. 1 (color). (a) A 3ω interaction beam is aligned along the axis of a gas-filled hohlraum where 33 heater beams heat the CH gas to a maximum electron temperature of 3.5 keV. (b) The electron temperature at the center of the hohlraum is measured using Thomson scattering where the total heater beam energy has been scaled from 8 kJ (circles) to 17 kJ (squares); the measurements are reproduced by hydrodynamic simulations (curves). (c) The calculated electron density along the interaction beam path at peak electron temperature is shown.

Facility [4]. The electron temperature along the interaction beam path is controlled by varying the heater beam energy from a maximum of 17 kJ; the plasma conditions along the interaction beam path have been measured using Thomson scattering [Figs. 1(b) and 1(c)] validating two-dimensional HYDRA [5] hydrodynamic simulations that show a uniform 1-mm plasma with a peak electron temperature of 3.5 keV [3]. These results provide confidence in the hydrodynamic parameters used as the foundation for laser-plasma interaction modeling. The interaction experiments are performed in the uniform density plateau [Fig. 1(c)] and before the shock waves driven by laser-beam ablation at the gold wall reach the hohlraum axis, around $t \simeq 1.3$ ns (stagnation) [6].

This new target platform together with a recently commissioned suite of laser-plasma interaction diagnostics [7,8] allows the access to high-temperature, long-scale length conditions not previously available using gasbag [9,10], toroidal hohlraum [11,12], or gas-filled hohlraum targets. Laser-plasma interaction thresholds are sensitive to the electron temperature and the length of the density plateau in a plasma; electron temperatures in open geometry gasbag plasmas with roughly the same plasma conditions are significantly lower than the target platform presented while scale lengths were much shorter in previous hohlraum platforms.

Gold 1.6-mm diameter, 2-mm long hohlraum targets produce a uniform density plateau using 1 atm of gas fill consisting of 30% CH_4, and 70% C_3H_8 expressed as partial pressures. The heater beams (1 ns square pulse) are focused near the 800 μm diameter laser entrance holes. The plasma conditions along the interaction beam path ($T_e = 3.5$ keV, $n_e = 5 \times 10^{20}$ cm^{-3}) are comparable to the current ignition targets planned to be shot on the National Ignition Facility.

The 3ω interaction beam (1 ns square pulse) is focused by a $f/6.7$ lens through a continuous phase plate [13] to a minimum vacuum diameter at the center of the hohlraum of 100 μm. The power averaged intensity at best focus for this beam is $I_p = E[J] \times 10^{13}$ W cm^{-2}, where E is the incident laser-beam energy ranging from 100 to 400 J.

Light scattered from the interaction beam is measured using a full-aperture backscatter station (FABS), near backscatter imager (NBI), and a 3ω transmitted beam diagnostic (3ωTBD) [7]. Light scattered back into the original beam cone is collected by the FABS; both the stimulated Brillouin scattering (SBS) and the stimulated Raman scattering (SRS) spectrum and energy are independently measured. Backscattered light outside of the original beam cone reflects from a plate surrounding the interaction beam. The plate is imaged onto two charge-coupled devices (CCD) which time integrate the SBS and SRS signals. In this study, the error in the measurements of the SBS power is 20%. The 3ωTBD allows us to accurately measure the light propagating through the target up to twice the original beam cone. The transmitted energy, spectrum, and temporal beam spray are measured. By correlating the plasma parameters, backscatter, and transmission measurements we are able to obtain a detailed scaling of reflectivity as a function of electron temperature.

Figure 2 shows a strong reduction in the backscattered light (<1%) as the electron temperature along the hohlraum axis exceeds 3 keV. The decrease in reflectivity with increasing temperature is a direct result of reducing the SBS three wave coupling as evident in the linear gain for intensity,

$$G_{\mathrm{sbs}} = 290\lambda_0[\mu\mathrm{m}]\left(\frac{n_e}{n_{\mathrm{cr}}}\right)\left(\frac{L[\mathrm{mm}]}{T_e[\mathrm{keV}]}\right)\left(\frac{\omega_a}{\nu_a}\right)I_{15}[\mathrm{W\,cm^{-2}}], \quad (1)$$

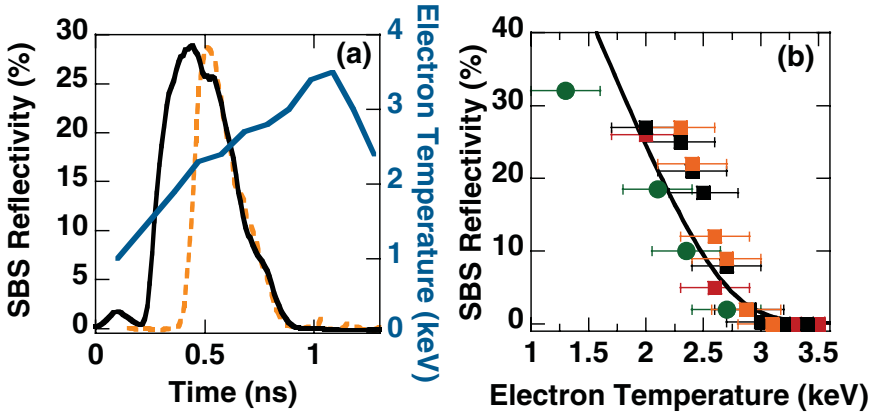

FIG. 2 (color). (a) The instantaneous SBS reflectivity (black, left axis) and electron temperature (blue, right axis) are plotted as a function of time for an intensity of $I_p = 2 \times 10^{15}$ W cm^{-2} and 14.5 kJ of heater beam energy. A second shot where the interaction beam was delayed by 200 ps (dashed orange line) produces the same instantaneous SBS reflectivity when the intensities are equal. This allows us to relate the SBS reflectivity to the electron temperature as shown in (b). Each point represents an average over 200 ps and each color corresponds to a separate shot; the total heater beam energy is varied from 8 kJ (circles) to 16 kJ (squares). As the electron temperature reaches 3 keV, the SBS backscatter drops below detection levels (< 1%).

where $\frac{n_e}{n_{cr}} = 0.06$ is the fraction of electron density to the critical density for 3ω light and $L \sim 1$ mm is the plasma length. T_e/T_i changes by less than 15% and the Landau damping (ν_a) normalized to the ion-acoustic frequency (ω_a) for our conditions is $\nu_a/\omega_a \approx 0.15$. The theoretical curve in Fig. 2(b) is obtained by applying linear theory including pump depletion [14],

$$R(1-R) = \epsilon e^{G_o(T_o/T_e)(1-R)}, \tag{2}$$

where $\epsilon \approx 10^{-9}$ is the thermal noise. The peak linear SBS gain calculated by postprocessing the plasma properties from HYDRA simulations using the code LIP [15] is $G_o = 28$ for $T_o = 1.8$ keV. At this intensity ($I_p = 2 \times 10^{15}$ W cm^{-2}) no backscattered light was detected by the NBI outside of the original beam cone. No SRS is measured in these experiments, as predicted by the moderate linear SRS gains ($G_{\mathrm{srs}} < 20$).

The SBS spectra measured by FABS [Fig. 3(a)] shows a narrow feature that peaks when the interaction beam reaches maximum power and the plasma is relatively cold ($T_e = 1.8$ keV). The temporal reflectivity and wavelength shift of this spectra are well reproduced by the linear gain calculations shown in Fig. 3(b) where the SBS power spectrum has been calculated using linear theory, Eq. (2). The simulated reflectivity is consistent with the measurements when the Gaussian instrument function ($\sigma = 100$ ps) has been convolved to account for the time smear introduced by the spectrometer. Both the simulation and the experimental results show that when the plasma reaches a temperature above 3 keV, the total backscatter is less than 1%.

Furthermore, the simulated SBS frequency shift is consistent with the measured spectrum when correcting for the frequency change observed in the forward scattered light [16]. Because the plasma density through which the light is propagating is increasing in time, the light frequency is upshifted [17]. Thus, the transmitted light is blueshifted by a few angstroms over the time of the experiment [18]. The SBS reflected light also experiences this upshift.

Low backscatter and high electron temperature leads to a peak transmission (Fig. 4) greater than 90% for intensities $I_p \leq 2 \times 10^{15}$ W cm^{-2}. The total scattered power (3ωTBD + backscatter) compares well with HYDRA simulations that account for inverse bremsstrahlung absorption.

In addition to this high transmission, Fig. 5 shows that 75% of the total transmitted power is measured within the original ($f/6.7$) beam cone after propagation through the high-temperature plasma. For intensities above $I_p > 2.0 \times 10^{15}$ W cm^{-2}, peak transmission within twice the beam cone drops to 70% and greater than 35% of the energy is outside of the original beam cone. Furthermore, backscattered light outside of the FABS is measured by the NBI. For the highest intensity shots (4×10^{15} W cm^{-2}), 50% of the total backscattered energy is outside of the original beam cone.

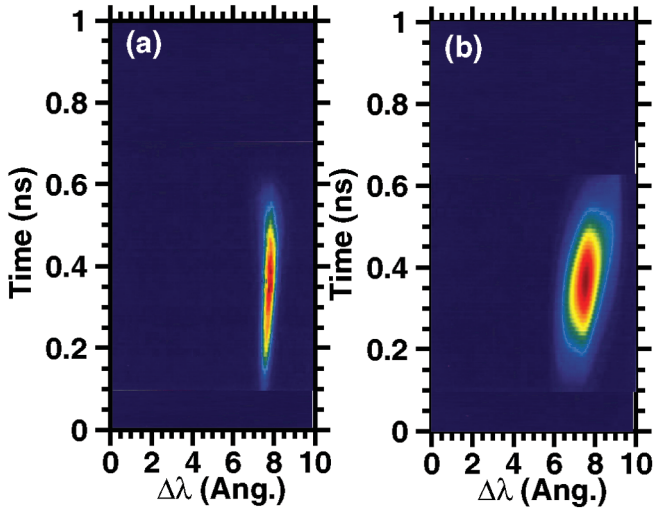

FIG. 3 (color). (a) The measured time-resolved SBS spectra for an intensity of $I_p = 2 \times 10^{15}$ W cm^{-2} and 15.5 kJ of heater beam energy is shown. (b) A synthetic SBS spectrum is obtained by postprocessing detailed hydrodynamic simulations with LIP and Eq. (2). The good agreement between these spectra confirms that SBS comes from the central density plateau. The wavelength shift ($\Delta\lambda = 7.5$ Å) is consistent with the simulated electron temperature ($T_e = 1.5$ keV) during the first 200 ps of the experiment.

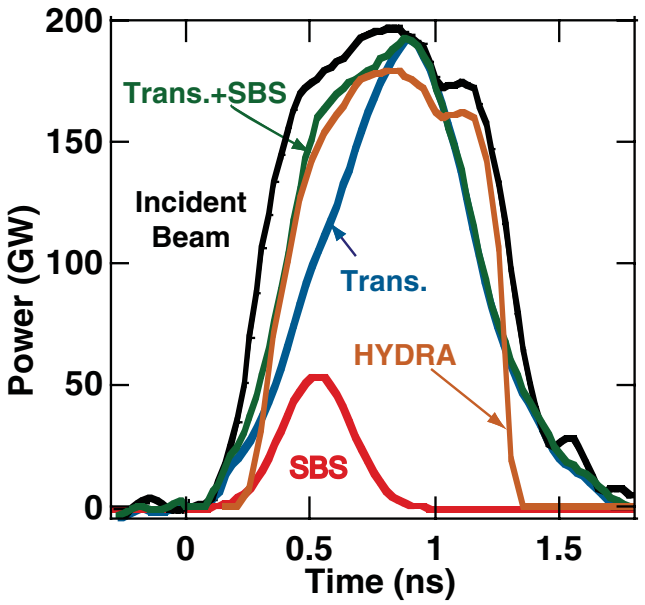

FIG. 4 (color). The time-resolved measured (blue) and calculated (orange) transmitted power is shown for conditions similar to those of Fig. 3. As HYDRA does not include backscatter, we add the measured SBS power (red) to the measured transmitted power (blue) and obtain the green curve which compares well. The incident beam power is shown in black. At peak electron temperature ($t = 900$ ps), we measure a peak transmission above 90%.

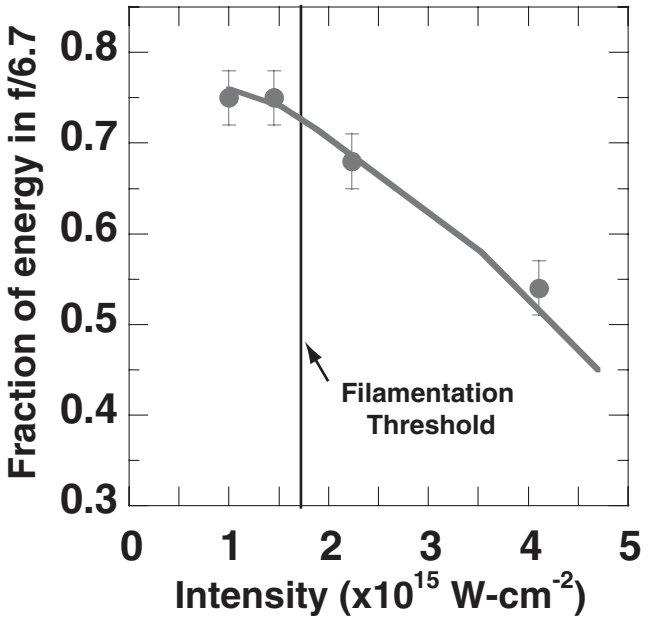

FIG. 5. The energy remaining inside of the original $f/6.7$ beam cone after propagation through the plasma is measured (circles) as a function of the interaction beam intensity. For intensities less than I_{FFOM}, more than 75% of the energy is measured to remain in the original $f/6.7$ beam cone.

Beam spray is a direct measure of filamentation; the filamentation threshold for an ideal beam can be calculated by balancing the plasma pressure with the ponderomotive force resulting from the transverse profile of the laser beam [19]. Theoretical work using the laser-plasma interaction code PF3D has extended this work to include the laser-beam intensity profile with a continuous phase plate [20],

$$\mathrm{FFOM} = \frac{I_p \lambda_0^2}{10^{13}} \left(\frac{n_e}{n_{\mathrm{cr}}}\right) \left(\frac{3}{T_e}\right) \left(\frac{f^{\#}}{8}\right)^2, \tag{3}$$

where I_p is the power averaged intensity at best focus, λ_0 is the wavelength of the laser beam, $n_e/n_{\mathrm{cr}} = 6\%$ is the fraction of electron density to the critical density at 3ω, $T_e = 3.5$ keV is the electron temperature, and $f^{\#} = 6.7$ is the ratio of the focal length to the beam diameter. When the filamentation figure of merit (FFOM) is greater than one, the beam is expected to experience significant filamentation and beam spray. Our measurements presented in Fig. 5 are compared with the peak FFOM determined by post-processing the parameters calculated by the hydrodynamic simulations where the filamentation threshold is calculated to be at $I_{\mathrm{FFOM}} = 1.7 \times 10^{15}\ \mathrm{W\,cm^{-2}}$; at intensities less than this threshold, more than 75% of the energy remains in the original beam cone. Thermal filamentation is not expected to significantly contribute as the electron mean free path is much greater than the transverse speckle size [21].

In summary, we have demonstrated laser-beam propagation through ICF hohlraums at ignition plasma conditions. This is accomplished through high electron temperature plasmas that keep laser-plasma instabilities below their linear thresholds ($G_{\mathrm{sbs,srs}} < 20$, FFOM < 1). For electron temperatures above 3 keV, the plasma is transparent, with transmission greater than >90% and less than <1% backscatter. Furthermore, the laser beam is shown to propagate without beam spray for intensities below $2 \times 10^{15}\ \mathrm{W\,cm^{-2}}$; above this intensity the beam is shown to filament. These experiments verify the ability of current models to predict ignition hohlraum conditions and laser-plasma interaction linear gains for filamentation, SBS, and SRS. The results show the importance of predicting the electron temperature when conditions are near backscatter thresholds; a small change in the electron temperature can lead to a significant increase in the backscattered energy.

We would like to acknowledge the efforts of the Omega Laser Crew. We thank D. Berger for his contributions. This experiment was made possible by D. Hargrove, V. Rekow, J. Armstrong, K. Piston, R. Knight, S. Alverez, R. Griffith, and C. Sorce with their contributions to the 3ωTBD. We thank R. Wallace and his fabrication team for the reliable targets. This work was supported by LDRD No. 06-ERD-056 and performed under the auspices of the U.S. Department of Energy by the Lawrence Livermore National Laboratory under Contract No. W-7405-ENG-48.

*Electronic address: froula1@llnl.gov
†Also at Engineering Department, University of Pacific, 3601 Pacific Avenue, Stockton, CA 95211, USA.

[1] J. D. Lindl *et al.*, Phys. Plasmas **11**, 339 (2004).
[2] W. L. Kruer, *The Physics of Laser Plasma Interactions* (Addison-Wesley Publishing Company, Inc., Reading, MA, 1988).
[3] D. H. Froula *et al.*, Phys. Plasmas **13**, 052704 (2006).
[4] J. M. Soures *et al.*, Laser Part. Beams **11**, 317 (1993).
[5] M. M. Marinak *et al.*, Phys. Plasmas **8**, 2275 (2001).
[6] S. H. Glenzer *et al.*, Phys. Plasmas **6**, 2117 (1999).
[7] D. H. Froula *et al.*, Rev. Sci. Instrum. 77, 10E507 (2006).
[8] A. J. MacKinnon *et al.*, Rev. Sci. Instrum. **75**, 3906 (2004).
[9] B. MacGowan *et al.*, Phys. Plasmas **3**, 2029 (1996).
[10] J. Moody *et al.*, Phys. Plasmas **7**, 3388 (2000).
[11] J. C. Fernandez *et al.*, Phys. Rev. Lett. **81**, 2252 (1998).
[12] B. H. Failor *et al.*, Phys. Rev. E **59**, 6053 (1999).
[13] S. Dixit *et al.*, Opt. Lett. **21**, 1715 (1996).
[14] C. Tang, J. Appl. Phys. **37**, 2945 (1966).
[15] E. A. Williams, UCRL Report No. UCRL-LR-105820-98, 1998.
[16] N. B. Meezan *et al.*, Phys. Plasmas (to be published).
[17] T. Dewandre *et al.*, Phys. Fluids **24**, 528 (1981).
[18] D. H. Froula, Phys. Plasmas (to be published).
[19] P. Kaw *et al.*, Phys. Fluids **16**, 1522 (1973).
[20] E. A. Williams, Phys. Plasmas **13**, 056310 (2006).
[21] C. Niemann *et al.*, Phys. Rev. Lett. **94**, 085005 (2005).